Chinese Chemical Letters 31 (2020) 2245–2248

Contents lists available at ScienceDirect

Chinese Chemical Letters

journal homepage: www.elsevier.com/locate/cclet

Communication

Melamine sponge derived porous carbon monoliths with NiMn oxides for high performance supercapacitor

Qianyuan Shan[a], Wangchen Huo[a], Man Shen[a], Chuan Jing[a], Yan Peng[b], Huayan Pu[a], Yuxin Zhang[a,*]

[a] State Key Laboratory of Mechanical Transmission, College of Materials Science and Engineering, Chongqing University, Chongqing 400044, China
[b] Research Institute of USV Engineering, Shanghai University, Shanghai 200444, China

ARTICLE INFO

Article history:
Received 2 January 2020
Received in revised form 29 January 2020
Accepted 5 February 2020
Available online 5 February 2020

Keywords:
NiMn oxides
Porous carbon
Supercapacito
Electrochemical performance
Melamine sponge

ABSTRACT

Supercapacitors with good electrochemical performance and flexibility are in great demand. In this paper, the concept of preparing 3D porous carbon monoliths via direct calcination of melamine sponge is presented. This preparation method is simple and has good control of the structure. Porous carbon composite nickel-manganese oxides can be obtained by hydrothermal method followed with calcination. The electrochemical performances were tested and porous carbon monoliths with NiMn oxides exhibited a specific capacitance of 870 F/g in 1 mol/L KOH at a charge/discharge current density of 0.5 A/g and a capacity retention of 89.9% after 5000 times charge and discharge.

With rapid development of portable electronic devices, electricity has gradually become the main form of energy used in people's daily lives [1]. As a key component of flexible, foldable and wearable electronic devices, energy storage materials also expected to have excellent flexibility and stability [2]. Supercapacitors has the potential to combine the advantages of both batteries and conventional and it can provide high energy density, power density and good cyclic stability [3]. As a kind of emerging battery-type electrode materials, transition metal oxides with unique layered structures, such as NiCo oxides, NiAl oxides, CoFe oxides and NiMn oxides have been widely investigated in the past few years for supercapacitors [4]. Among many metal oxides, nickel-manganese bimetal oxides have many unique advantages, including high theoretical specific capacitance, low price, rich natural reserves and simple synthesis. At the same time, nickel and manganese oxides have good synergistic effect and showed better performance than single metal oxides. However, the layered structure of NiMn oxides tend to re-stack together during charging and discharging, which lead to poor cyclic stability. Due to its limited conductivity, its electrochemical capacitance is far lower than theoretical value [5].

To make better use of the characteristics of NiMn oxides and make up for shortcomings, studies have reported the composition of NiMn Oxide with graphene, carbon nanotubes and other carbon materials with excellent conductivity [6–8]. As for the structure stability, by integrating NiMn oxides with hierarchical three-dimensional (3D) nanomaterials, these 3D nanomaterials can support NiMn oxides like a skeleton and prevent severe agglomeration [9]. Porous carbon has 3D interlaced network structure and has been used in batteries, oil removal, and heat insulators [10–12]. However, due to the high cost of preparation, complicated preparation process, the mass production of carbon monoliths with uniform structure is still a challenge [13,14]. Therefore, it is urgently needed to develop a low-cost and feasible method to prepare of 3D porous carbon monoliths to overcome the limitations.

Preparing porous carbon monoliths from commercially available melamine sponges is a viable method. As household cleaning pads commonly used in daily life, melamine sponge with 3D microporous structure have exhibited a high absorption capacity for both water and oil [15,16]. Commercial sponges have the features of low density (3–10 mg/cm^3), high porosity (over 99%), robustness, good elasticity, and flexibility [17]. According to the molecular formula ($C_6H_9N_6$) of melamine sponge, it has high content of N atoms and H atom and is a perfect starting material to fabricate various devices.

Therefore, in this study nickel-manganese layered double hydroxide was first grown on the sponge. Then, the 3D structured porous carbon-supported NiMn oxides was obtained by calcination. This composite has a stable structure, excellent electrical

* Corresponding author.
E-mail address: zhangyuxin@cqu.edu.cn (Y. Zhang).

https://doi.org/10.1016/j.cclet.2020.02.003
1001-8417/

conductivity and electrochemical performance. Benefiting from the sophisticated structure and components, the optimized carbon/NiMn oxides delivers excellent performance.

As shown in Fig. 1, NiMn LDH nanosheet were prepared on melamine sponge by co-deposition and calcination. Specifically, 3 mmol $Ni(NO_3)_2{\cdot}6H_2O$ (98 wt%), 1 mmol $Mn(NO_3)_2{\cdot}H_2O$ aqueous solution (50 wt%) and 13.2 mmol urea were desolved into 70 ml of deionized water with magnetic stirring, which form a transparent green solution. A sponge with the size of $0.5\times2\times7$ cm^3 was washed with distilled water and ethanol respectively. The sponge was then placed in the solution and heated at 80 °C for 6 h. After the water bath, the sponge with NiMn LDH nanosheets was taken out, washed several times with excess dionized water and dried in air at 60 °C. The as-prepared NiMn LDH on melamine sponge was labeled as NiMn-1. The NiMn oxide was prepared by annealing NiMn-1 at 350 °C for 2 h. At this temperature, sponge was carbonized and carbon skeleton with NiMn oxide nanosheets was prepared, marked as C-NiMn-1. At the same time, the metal ratio at a total concentration of 4 mmol and the ratios (Ni^{2+} and Mn^{2+}) were 1:1, 1:3 were prepared under the same condition, named as C-NiMn-2, C-NiMn-3.

The chemical compositions and crystallography information of as-prepared samples were identified by powder X-ray diffraction (XRD, D/max 2500, Cu Kα). The structures and morphologies were characterized by focused ion beam scanning electron microscopy (FIB/SEM, ZEISS AURIGA). The electrochemical tests were performed on a three-electrode system using CH Instruments CHI660E. This three-electrode system use NiMn oxides as working electrode, a platinum plate as counter electrode and a saturated calomel electrode (Hg/HgO) as the reference electrode. The specific capacitance of active materials was measured by galvanostatic charge-discharge measurements using the following equation:

$$C_s = I\Delta t/m\Delta U$$

where I (A) is discharge current, Δt (s) is discharge time, ΔU (V) is the voltage difference of the discharge and m (g) is the total mass of active material.

The microstructures of the samples were investigated using SEM, as shown in Fig. 2. The interconnected nanosheets homogeneously grown on sponge fibers. The diameters of sponge fibers are around several microns, while the thickness of nanosheets are tens of nanometers. With the increase of $Mn(NO_3)_2$ during the preparation, the nanosheets became denser and more irregular. The inset photos show the sponge-LDH and with the increase of Mn^{2+}, the color of products changes from light green to brown. As $Mn(OH)_2$ are in the color of dart brown. From the SEM image with higher magnification on the right side, it can be observed that the nanosheets of sample C-NiMn-1 are thinner, the layers are staggered with each other and enough space are left, so that electrolyte can fully wet the NiMn oxide surface. This structure can effectively increase active area thus improve electrochemical performance. As the content of manganese increases, the thickness of lamella gradually increases, and the space between lamella decreases accordingly. When the content of nickel and manganese is 1:3, the growth of lamellae is much denser and there is almost no gap between lamellae. This has a negative effect on the progress of the electrochemical reaction.

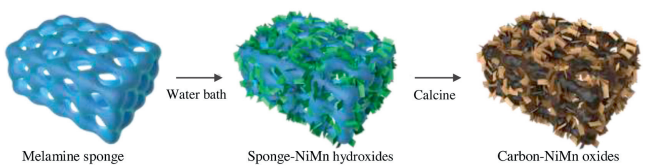

Fig. 1. Schematic illustration ofpreparation process of carbon-NiMn oxides.

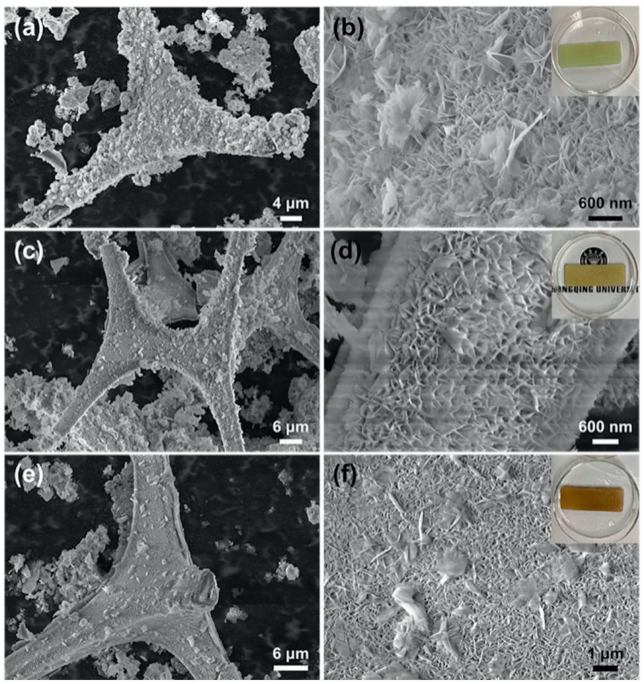

Fig. 2. SEM images of (a, b) C-NiMn-1, (c, d) C-NiMn-2, (e, f) C-NiMn-3 at different magnifications.

The crystal structures of different samples were investigated by XRD. As shown in Fig. 3a, the diffraction peaks can be indexed to a serious of crystal planes, demonstrating a successful preparation of NiMnLDH [18]. The strong peaks in Fig. 3a belong to $Ni(OH)_2$. The peaks at 2θ values of 11.3°, 22.7°,34.4°, 38.8° and 60.0° were indexed to (003), (006), (012), (015), (110) from the standard data (JCPDS No. 38-0714).The samples prepared with different Ni and Mn ratio showed peaks at slightly different position and intensity. After calcination, the oxidized NiMn LDH was transformed into NiMn oxides. Fig. 3b showed the XRD pattern of electrode materialsafter calcination. it confirmed the formation of nickel manganese oxide (JCPDF No. 01-1110). It could be observed that diffraction peaks of 37.3°, 43.3°, and 57.2° corresponded to the (222), (400), (440) planes. The wide peak at 27° belonged to the porous carbon [19]. As mentioned above, all the electrode materials were synthesized successfully. The pore structures of NiMn-1 and C-NiMn-1 were investigated by N_2 adsorption-desorption isotherms (Fig. S1 in Supporting information). The NiMn-1 shows typical type-IV isotherms. The C-NiMn-1 exhibits type-I isotherms with a hysteresis loop at high relative pressure, suggesting a mainly microporous structure.

In order to better study the electrochemical properties of the composite materials, the tests were performed on materials before and after calcination. Fig. S2 (Supporting information) is the GCD, CV and Nyquist plot of non-calcined sponge supported NiMn hydroxide. It can be observed that it has limited capacitance provided by NiMn hydroxide. When the current density is 0.5 A/g, the specific capacitance is about 135 F/g. With the increase of current density, the specific capacitance decreases. Nyquist plots in Fig. S2c (Supporting information) showed large semi-circle, which indicate large internal resistance due to the existence of sponge.

After calcination under 350 °C for 2 h, the sponge was carbonized into three-dimensional porous carbon and NiMn hydroxide was oxidized into NiMn bimetal oxides at high temperature. To further study the influence of molar ratio of Ni and Mn on the electrochemical performances, samples with the Ni, Mn ratios of 3:1 (C-NiMn-1), 1:1 (C-NiMn-2) and 1:3 (C-NiMn-3)

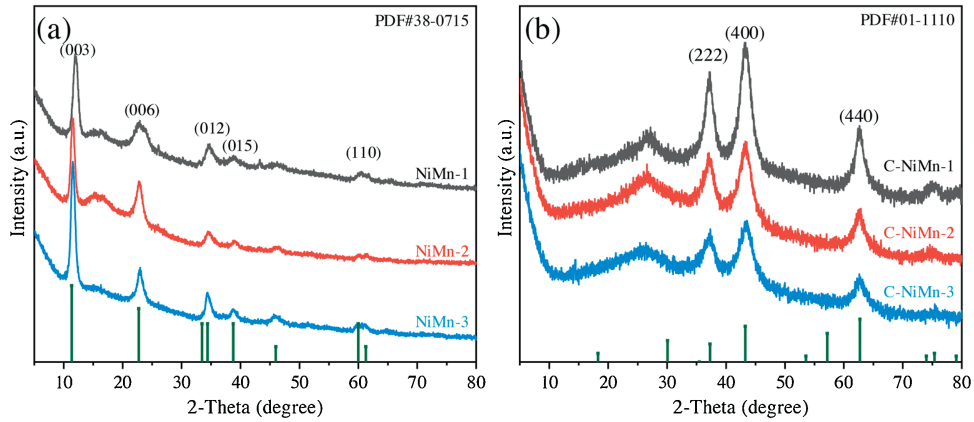

Fig. 3. XRD patterns of (a) sponge-NiMn hydroxide samples and (b) porous carbon-NiMn oxides.

were prepared and tested (Fig. S3 in Supporting information). Compared with C-NiMn-2 and C-NiMn-3, C-NiMn-1 has longer charge and discharge time under the same current density, which means that C-NiMn-1 can store and release more electrical energy. The cyclic voltammetry tests also showed the same results. The area enclosed by CV curves of C-NiMn-1 was larger than the other two. The electrochemical tests showed that when the ratio of Ni to Mn is 3:1, it has the best performance. The redox peaks of C-NiMn samples are located at the same voltage ranges compared with the literature. For C-NiMn-1, there is a pair of redox peaks located at 0.19 and 0.51 V when the scan rate was 0.1 V/s, corresponding to the reversible Faradaic reaction in alkaline solution. The redox reaction of electrode can be expressed by the following formula:

$$NiO + OH^- \leftrightarrow NiOOH + e^-$$

$$MnOOH + OH^- \leftrightarrow MnO_2 + H_2O + e^-$$

In the potential range of 0-0.6 V, paired redox peaks appear in the cyclic voltammetry curves. As the scan rate increases, the redox current increases, and the relative potential of the redox peaks shifts slightly, indicating that the redox reaction of NiMn oxides is reversible.

The specific capacitances of C-NiMn samples at different current densities were calculated by galvanostatic charge-discharge measurements. The calculation results are shown in Fig. 4a. As the current density increases, part of the active materials cannot fully participate in the electrochemical reaction, resulting in a decrease in specific capacitance. The notably large specific capacitance of 870 F/g at current density of 0.5 A/g compare to 590 and 350 F/g of C-NiMn-2 and C-NiMn-3. At high current density of 10 A/g, the specific capacitance of C-NiMn-1 is 540 F/g, indicating capacitance retention of 62%. As a pseudo capacitor, the energy storage process occurs on both the surface and bulk phase of the electrode materials. The larger the specific surface area, the more electrochemically active site can be provided for redox reaction, so that more electric charges are stored in the electrode materials and redox reaction can be carried out more efficiently. While the specific capacitance of all three materials decreases with the increase of current density, C-NiMn-1 has better performance than the other two due to it large specific surface area and suitable chemical composition.

The electrochemical impedance spectroscopy was used to test the internal resistance of C-NiMn oxides. The electrochemical impedance $Z(\omega)$ is defined as $Z(\omega) = \Delta V/\Delta I = |Z(\omega)|e\text{-}j\varphi = Z' + jZ''$, where Z' and Z'' are the real part and the imaginary part of the impedance, respectively, defined as $Z'^2 + Z''^2 = |Z(\omega)|^2$ [20]. The difference in the active materials in the electrode leads to a difference in the resistance from one electrode to the other. The high-frequency resistance is greatly decreased after calcination. Before calcination (Fig. S2c in Supporting information), the electrode is composed of melamine sponge and nickel manganese dioxide. Melamine sponge is a non-conductive substance, so the resistance of the electrode is relatively high. After calcination at a suitable temperature (Fig. 4b), melamine sponge is carbonized into porous carbon. This porous carbon has an interconnected three-dimensional structure and has good electrical conductivity, so the internal resistance is significantly reduced.

After 5000 cycles, C-NiMn-1 retained 89.9% of the initial capacitance, which indicate that the staggered NiMn oxide nanosheets with 3D porous carbon monoliths as scaffolds have good stability (Fig. 4c). The C-NiMn-3 showed capacity drop of 81.7%, which is higher than C-NiMn-1. As we can see from the SEM images, C-NiMn-3 nanosheets densely packed together, leaving

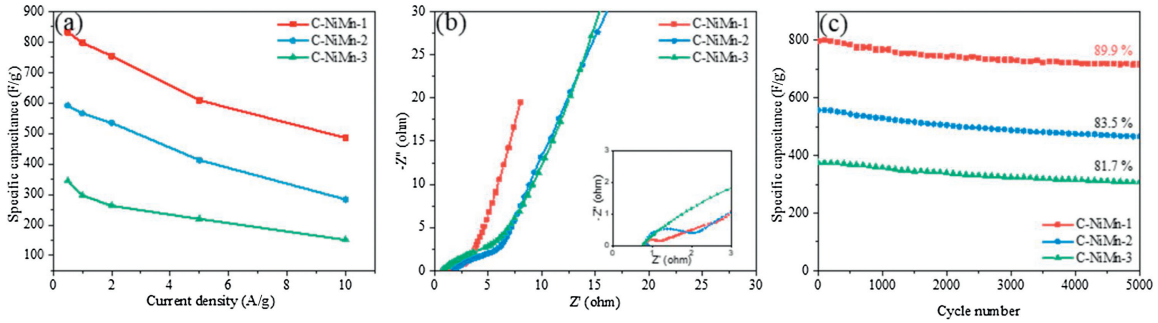

Fig. 4. (a) Comparison of the specific capacities as a function of current density. (b) The Nyquist plots in the frequency range of 0.01–100 kHz. (c) The cyclic stability of C-NiMn samples.

limited space for structure expansion and contraction. During the insertion and desorption of electrolyte ions into the metal oxides matrix, the expansion and shrinkage of the composite may cause loss of active materials and cracks between electrode and current collector. This would greatly influence the cyclic stability.

In conclusion, the preparation of porous carbon with NiMn oxides by the direct carbonization of melamine form with precursor is demonstrated. Porous carbon monolith prepared by melamine foam has the advantages of light weight, high porosity, and stable structure. The growth of NiMn oxide ultrathin nanosheets can greatly increase the active reaction area and ensure good cycle stability. The as prepared electrode materials exhibited specific capacitance of 870 F/g at current density of 0.5 A/g and a good cyclic stability of 89.9% after 5000 times charge and discharge. Moreover, the inexpensive raw materials of melamine foam and simple preparation process ensure that the large-scale production of C-NiMn oxides can be implemented easily.

Declaration of competing interest

The authors declare that they have no known competing financial interests or personal relationships that could have appeared to influence the work reported in this paper.

Acknowledgments

This work received financial support from the National Natural Science Foundation of China (Nos. 21576034 and 51908092), the State Education Ministry and Fundamental Research Funds for the Central Universities (Nos. 2019CDQYCL042, 2019CDXYCL0031, 2018CDYJSY0055, 2018CDQYCL0027, 106112017CDJQJ138802, 106112017CDJSK04XK11 and 106112017CDJXSYY0001), the Joint Funds of the National Natural Science Foundation of China-Guangdong (No. U1801254). The authors thank the Electron Microscopy Center, Analytical and Testing Center of Chongqing University for materials characterizations.

Appendix A. Supplementary data

Supplementary material related to this article can be found, in the online version, at doi:https://doi.org/10.1016/j.cclet.2020.02.003.

References

[1] E. Pomerantseva, F. Bonaccorso, X. Feng, Y. Cui, Y. Gogotsi, Science 366 (2019) 969.
[2] L. Jin, R. Gong, W. Zhang, J. Mater. Chem. A 7 (2019) 8234–8244.
[3] S. Chen, G. He, H. Hu, et al., Energy Environ. Sci. 6 (2013) 2435–2439.
[4] Y. Liu, D. Zhao, H. Liu, A. Umar, X. Wu, Chin. Chem. Lett. 30 (2019) 1105–1110.
[5] A. Sumboja, J. Chen, Y. Zong, P.S. Lee, Z. Liu, Nanoscale 9 (2017) 774–780.
[6] D. Zhao, H. Liu, X. Wu, Nano Energy 57 (2019) 363–370.
[7] Z. Liu, H. Song, Y. Zhao, et al., ACS. Mater. Lett. 1 (2019) 290–296.
[8] Q. Yu, Lv J, Z. Liu, et al., Sci. Bull. (Beijing) 64 (2019) 1617–1624.
[9] L. Yang, L. Chen, D. Yang, et al., J. Power Sources 392 (2018) 23–32.
[10] J. Du, L. Liu, Y. Yu, Y. Zhang, A. Chen, Chin. Chem. Lett. 30 (2019) 1423–1427.
[11] S. Chen, L. Zhao, J. Ma, et al., Nano Energy 60 (2019) 536–544.
[12] X. Gao, J. Feng, D. Su, et al., Nano Energy 59 (2019) 598–609.
[13] M. Xu, Q. Yu, Z. Liu, et al., Nanoscale 10 (2018) 21604.
[14] Y. Huang, Y. Wang, C. Tang, et al., Adv. Mater. 31 (2019) 1803800.
[15] J. Zhang, G. Chen, Q. Zhang, F. Kang, B. You, ACS Appl. Mater. Interfaces 7 (2015) 12760–12766.
[16] Z. Lei, P. Zheng, L. Niu, et al., Appl. Surf. Sci. 489 (2019) 922–929.
[17] S. Qiu, B. Jiang, X. Zheng, et al., Carbon 84 (2015) 551–559.
[18] W. Huang, A. Zhang, X. Li, et al., J. Power Sources 440 (2019) 227123.
[19] L. Jin, X. Guo, R. Gong, et al., Energy Storage Mater. 23 (2019) 409–417.
[20] P.L. Taberna, P. Simon, J.F. Fauvarque, J. Electrochem. Soc. 150 (2003) A292–A300.